Journal of
*Composites Science*

MDPI

*Article*

# Modification of Bitumen with Graphene Oxide-like Material from Lemon Peel Biochar via a Modified Hummers Method

**Aliya Kenzhegaliyeva [1] and Yerdos Ongarbayev [1,2,*]**

[1] Institute of Combustion Problems, 172, Bogenbai Batyr Str., Almaty 050012, Kazakhstan; aliakenzik@gmail.com
[2] Faculty of Chemistry and Chemical Technology, Farabi University, 71, Al-Farabi Ave., Almaty 050040, Kazakhstan
* Correspondence: erdos.ongarbaev@kaznu.edu.kz; Tel.: +7-7014575789

**Abstract**

This study examined the effect of a graphene oxide-like (GO-like) carbon material obtained from lemon peel biochar on road bitumen. Pyrolysis of the raw material was conducted at 500, 550 and 600 °C. The graphene oxide-like carbon material was synthesized using a modified Hummers method. Among the investigated pyrolysis temperatures, 550 °C produced the most favorable structural characteristics, including a higher contribution of oxygen-containing groups and a more uniform structure. Adding a selected dosage of 3 wt.% graphene oxide-like carbon material increased shear stress by 20–25 kPa, ultimate strain from 13 to 17%, and fatigue life by 36–109%. The results confirm the potential of using lemon peel biochar to produce a road bitumen modifier.

**Keywords:** bitumen; graphene oxide-like carbon material; modified Hummers method; biochar; waste valorization

## 1. Introduction

The development of transport infrastructure requires improved durability and performance characteristics of road surfaces. Traditional petroleum bitumen used as a binder for asphalt concrete mixtures has several drawbacks, including low rutting resistance at high temperatures and a susceptibility to fatigue failure and aging during service [1]. One of the current areas of research is the modification of bitumen with various additives capable of improving its rheological and mechanical properties [2]. Recent studies have shown that nanoscale characteristics of bitumen determined by AFM can be significantly influenced by thermal history and sample preparation conditions [3].

In recent years, particular attention has been paid to the use of carbon nanomaterials, with graphene oxide of particular interest. Due to its two-dimensional structure, high specific surface area, and the presence of oxygen-containing functional groups, graphene oxide is able to effectively interact with bitumen components, forming a more stable and durable binder structure [4].

Graphene oxide can significantly increase the surface free energy of bitumen and reduce the effects of aging on this parameter. GO also improves adhesion between bitumen and mineral aggregate, as well as the moisture resistance of the asphalt concrete mixture [5].

The results showed that GO increases the high-temperature stability and resistance of bitumen to thermal aging but does not improve its crack resistance. GO is stably dispersed in bitumen, forming an intercalation structure, which enhances the high-temperature



Academic Editor: Zengping Zhang

Received: 12 August 2026
Revised: 9 September 2026
Accepted: 14 September 2026
Published: 16 September 2026

stability of the material. However, the effect of GO on bitumen is a physical modification: the components do not form chemical cross-links with each other, as a result of which the crack resistance of the modified bitumen does not increase [6].

A previous study [7] showed that the combined use of graphene oxide with warm-mix asphalt concrete additives improves the properties of modified bitumen binders. The combination of GO and Sasobit R increases the material's resistance to high-temperature deformation, while the combination of GO with waste vegetable oil improves its fatigue life and low-temperature properties.

The most common method for synthesizing graphene oxide is the Hummers method, based on the oxidation of graphite with strong oxidizing agents in an acidic medium [8]. The resulting material has a layered structure and contains a large number of oxygen-containing groups, which ensures good dispersibility in various matrices and promotes effective interaction with organic materials [9].

Growing interest in producing carbon materials from renewable raw materials and biomass contributes to solving environmental waste disposal problems [10,11]. Recent research also demonstrates the potential of agricultural byproducts as bitumen modifiers. For example, olive seed powder was investigated as a biopolymer modifier using physicochemical and rheological methods, confirming the growing interest in using biomass waste to modify bitumen binders [12]. Lemon peel and other citrus peels are promising carbon-rich biomass precursors that can be converted into porous carbon structures through carbonization and subsequent activation [11,13,14]. For example, activated microporous carbon was successfully obtained from lemon peel by carbonization followed by $CO_2$ activation. This confirms the suitability of lemon peel biomass as a carbon precursor and demonstrates that controlled thermal processing enables the production of carbon materials with developed microporosity [14].

However, producing high-quality graphene oxide from biomass is associated with a number of technological challenges. Unlike natural graphite, biochar has a less ordered crystalline structure and contains non-carbon impurities, requiring optimization of carbonization and subsequent oxidation processes to achieve a degree of graphitization sufficient to form nanoscale sheets [15]. Implementing such solutions enables the transformation of organic waste into a high-tech product with added value.

A previous study [16] shows that pyrolysis temperature plays a dominant role in stimulating aromatization and graphite domain growth. Overall, controlled pyrolysis conditions are necessary for producing biochar from biomass with graphene-like carbon structures and for developing stable graphene precursors.

Graphene oxide (GO) is gaining increasing attention as a modifier for bitumen binders due to its high specific surface area, layered morphology, and the presence of oxygen-containing functional groups. Previous studies have shown that GO can modify the rheological behavior of bitumen, increase its stiffness and elasticity, and improve its resistance to permanent deformation. However, the magnitude of these effects depends significantly on the GO dosage, the type of starting bitumen, the preparation conditions of the modified binder, and the quality of dispersion [17,18].

The effect of GO on the fatigue behavior of bitumen has also been studied using modern rheological methods. Singh et al. [17] investigated GO contents in the range of 1–3 wt.% and reported improvements in both rutting resistance and fatigue performance, with the most favorable dosage varying depending on the parameter being evaluated. Similarly, studies using the LAS test with GO contents ranging from 0.5 to 2.5 wt.% showed an increase in fatigue life, demonstrating GO's ability to influence damage accumulation under cyclic shear loading [19]. These results also indicate that increasing GO content does not necessarily result in a proportional improvement in all asphalt binder properties.

The effect of GO on the aging behavior of bitumen has also been reported. Wu et al. [20] investigated GO contents of 1 and 3 wt.% and found differences in the physicochemical and rheological properties of binders after thermos-oxidative and ultraviolet aging, with the effect dependent on GO content and bitumen type. Other studies of carbon nanomaterials have also shown changes in rheological and fatigue properties after aging. However, the literature does not allow us to identify a single universal GO dosage or a single modification mechanism applicable to all types of asphalt binders [18]. A recent review paper [21] also highlighted that bitumen binders modified with graphene, graphene nanoplatelets, and GO generally exhibit promising rheological properties. However, significant variability remains among published results, particularly with regard to low-temperature properties, aging behavior, dispersion quality, and the proposed modification mechanisms. Furthermore, most studies utilized commercially available graphene materials obtained from traditional graphite feedstocks.

Meanwhile, carbon-containing materials from biomass are gaining increasing interest as alternative precursors for producing graphene-like and graphene-oxide-like materials.

Agricultural and biological wastes, including rice husks, sugarcane bagasse, wood pulp, and other carbon-rich residues, have been used to produce oxidized graphene-like materials using modified Hummers methods. These studies demonstrate that the nature of the feedstock and thermal processing conditions significantly influence the degree of structural ordering, defect density, content of oxygen-containing functional groups, and the final properties of the resulting material [15].

It is important to note that materials derived from biochar should not be considered structurally identical to traditional graphite-derived GO [22]. Direct comparative studies of graphite and biochar precursors have revealed differences in the degree of structural ordering, defect distribution, ratio of $sp^2$- and $sp^3$-hybridized carbon regions, and degree of crystallinity. Such differences, due to the nature of the feedstock, can potentially influence the behavior of the material when incorporated into complex matrices, including bitumen [23]. Despite the growing body of research on graphene oxide-modified bitumen binders and biomass-derived graphene-like materials, these two research streams remain largely separate. Most bitumen modification studies utilize commercially available GO or graphite-derived graphene oxide, while biomass-derived graphene-like materials are primarily being explored for environmental, electrochemical, and other functional applications. In particular, there is limited data on the preparation of graphene-oxide-like carbon materials from lemon peel biochar, as well as how the pyrolysis temperature of such a precursor affects its structural characteristics and subsequent properties as a bitumen modifier. Furthermore, the fatigue behavior of bitumen modified with such biomass-derived material after long-term oxidative aging has not yet been adequately studied using LAS/VECD analysis. Thus, the novelty of this study lies in the integrated approach, including the use of lemon peel waste as a carbon precursor, control of the precursor structure through pyrolysis at different temperatures, synthesis of a graphene-oxide-like material using a modified Hummers method, selection of the most favorable pyrolysis temperature based on Raman, AFM, and FTIR characterization data, and subsequent evaluation of the rheological and fatigue behavior of bitumen modified with the resulting material after long-term laboratory oxidative aging.

Accordingly, the aim of this study was to prepare a graphene oxide-like carbon material from lemon peel biochar using a modified Hummers method, evaluate the effect of biochar pyrolysis temperatures of 500, 550 and 600 °C on its structural and morphological characteristics, and investigate the rheological and fatigue properties of bitumen containing 3 wt.% of the selected material after long-term laboratory oxidative aging using LAS/VECD analysis.

## 2. Materials and Methods

The study utilized BND 100/130 grade road petroleum bitumen produced by the Pavlodar Petrochemical Plant (Pavlodar, Kazakhstan). The bitumen exhibits the following physicochemical properties: penetration at 25 °C of 129.6 ± 0.1 mm, softening point of 46.9 °C, and ductility at 25 °C of 111.6 cm.

Lemon peel was dried in an oven at 80 °C for 24 h to remove residual alcohol and water and then ground to micrometer size in a knife mill.

### 2.1. Synthesis of Biochar from Lemon Peel

The pyrolysis process was carried out in an electric furnace equipped with a cylindrical stainless-steel reactor that served as a sample holder (Figure 1). The geometric parameters of the reactor were: length—15 cm, internal diameter—5 cm. All the main parameters of the process, including temperature, heating rate and gas flow rate, were programmed and constantly monitored. About 20 g of a pre-prepared raw material–lemon peel sample was loaded into the reactor, and then heated to a temperature of 500, 550 or 600 °C. The pyrolysis duration was about 1 h. During the thermal treatment process, pure nitrogen was continuously supplied to the reactor, which prevented unwanted oxidation reactions and provided an inert atmosphere. After the experiment, the biochar was removed from the reaction chamber. All samples were synthesized under the same conditions, which ensured the comparability of the results obtained and allowed for a correct comparative analysis.

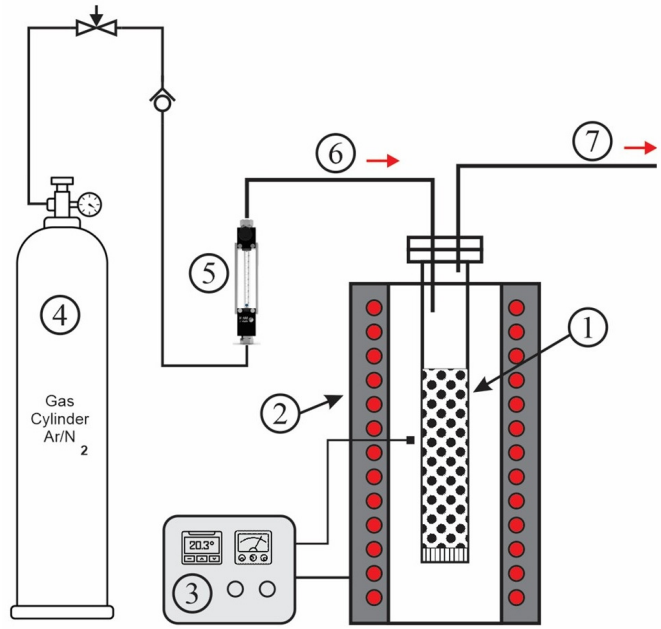


**Figure 1.** Schematic diagram of a biomass pyrolysis plant: 1—stainless steel reactor with inlet and outlet gas lines; 2—electric vertical tubular furnace; 3—temperature control unit; 4—inert gas tank (cylinder); 5—gas flowmeter (rotameter); 6—inlet line; 7—outlet line (volatile gases line).

### 2.2. Synthesis of Graphene Oxide from Biochar

The synthesis of graphene oxide-like material from biochar using a modified Hummers method is shown in Figure 2. Unlike the classical Hummers method [24], this procedure eliminates the use of sodium nitrate $NaNO_3$, preventing the release of toxic nitrogen oxides and making the method safer and more environmentally friendly. Phosphoric acid $H_3PO_4$ is also added, promoting gentler and more uniform oxidation, increasing interlayer spacing, and reducing defects in the graphene lattice.

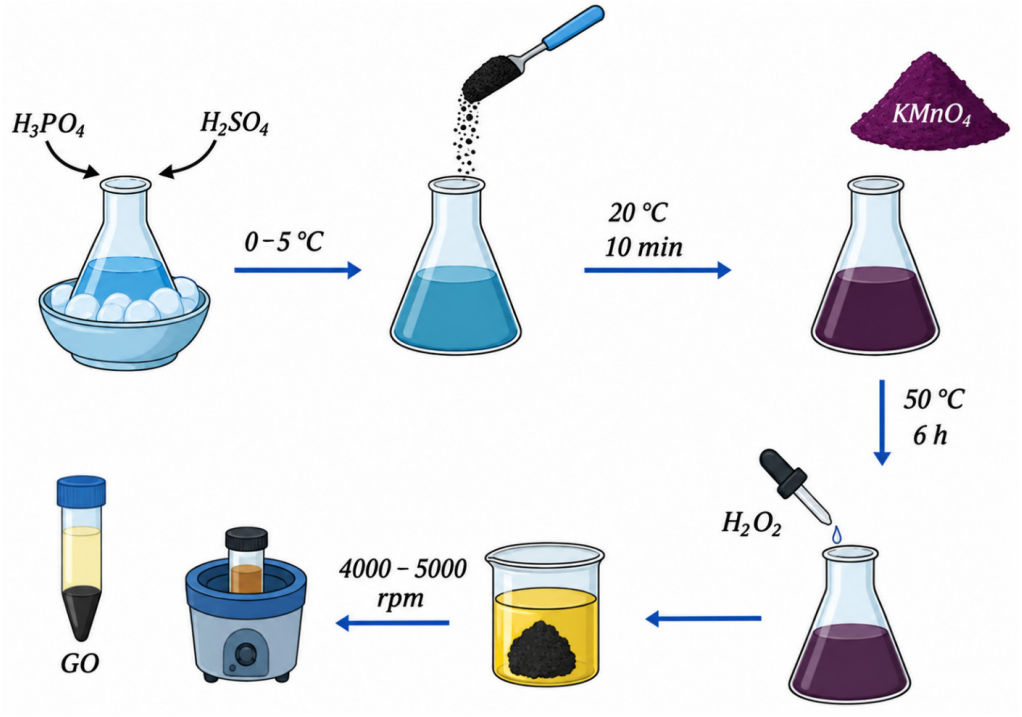


**Figure 2.** Schematic diagram of graphene oxide-like (GO-like) material synthesis from biochar using a modified Hummers method.

For 1 g of biochar, we used 6 g of potassium permanganate $KMnO_4$, 45 mL of concentrated sulfuric acid $H_2SO_4$ (98%), 5 mL of phosphoric acid $H_3PO_4$ (85%), 5–6 mL of hydrogen peroxide $H_2O_2$(30%), 200 mL of distilled water, and approximately 50 mL of a 5% hydrochloric acid HCl solution.

45 mL of $H_2SO_4$ and 5 mL of $H_3PO_4$, were poured into a dry, heat-resistant container, stirred, and cooled in an ice bath to a temperature of 0–5 °C. A total of 1 g of pre-crushed biochar was slowly added to the cooled acid mixture, maintaining the temperature no higher than 10 °C. After 10 min of stirring $KMnO_4$ was added portionwise, maintaining the reaction mixture temperature at $\leq$20 °C. After the oxidizer had been completely added, stirring was continued for another 10–15 min in the cold.

The reaction mixture was then heated to 50 °C and maintained at this temperature for 6 h with slow agitation. Once the oxidation was complete, the mixture was cooled to room temperature (~25 °C), after which 100 mL of cold distilled water was slowly added. Next, 5–6 mL of 30% hydrogen peroxide was added dropwise until a characteristic yellow-brown color appeared, indicating the removal of $Mn^{2+}$ ions.

The resulting suspension was transferred to centrifuge tubes and centrifuged at 4000–5000 rpm for 10–15 min. The precipitate, containing large fragments of graphene oxide-like material and residual $MnO_2$, was separated, and the supernatant was decanted. The precipitate was washed with distilled water 2–3 times until a pH of 6–7 was reached (as measured using universal indicator paper).

To isolate the graphene oxide nanofraction, the supernatant was further centrifuged at 7000–8000 rpm for 5–7 min. The resulting precipitate, containing finely dispersed graphene oxide sheets, was dispersed in 20–50 mL of distilled water and sonicated for 10–20 min to obtain a stable colloidal suspension. The resulting sample was stored at 4 °C. Prior to bitumen modification, the required amount of GO-like material was separated from the aqueous medium and dried to remove residual water. The dried GO-like material was then used for preparation of the modified bitumen.

### 2.3. Raman and Infrared Spectroscopy Analysis

Measurements were performed on a Solver Spectrum Raman spectrometer (NT-MDT BV, Amsterdam, The Netherlands) equipped with a 473 nm laser, which corresponds to the blue spectrum of the visible range. This wavelength was chosen to minimize sample fluorescence, which is especially important when analyzing organic and biological materials. The laser beam was focused on the sample surface using a 100× objective, providing high spatial resolution, which is critical when studying micro- and nanoscale structures.

To record the Raman signal, a diffraction grating with a density of 600 lines/mm was used, providing a spectral resolution of 4 $cm^{-1}$. This resolution allows for the detection of fine structural features and small shifts in the spectrum, which is important when analyzing complex materials. The signal accumulation time was 60 s, which is optimal for obtaining a high-quality spectrum with a good signal-to-noise ratio, especially when working with samples prone to fluorescence.

Using a 473 nm laser also enhances the Raman signal, as shorter wavelengths result in more intense scattering. However, it is important to note that when choosing a wavelength, it is important to consider the balance between signal enhancement and the potential occurrence of fluorescence, which can complicate spectrum interpretation.

Infrared spectroscopic (IR) analysis was carried out with a Bruker Alpha spectrometer (Bruker, Karlsruhe, Germany). The spectra were taken in the wavenumber range from 400 to 4000 $cm^{-1}$. Prior to comparing the intensities of the characteristic bands, all FTIR spectra were normalized to ensure a valid comparison of the samples and to minimize the influence of differences in overall signal intensity.

### 2.4. Atomic Force Microscopy Analysis

For the AFM analysis of the synthesized carbon material, an aqueous dispersion of the sample was deposited on freshly cleaved mica. Prior to deposition the dispersion was sonicated to improve particle dispersion. The deposited samples were dried before AFM measurement to remove residual water.

Atomic force microscopy was performed using a Solver Spectrum combined imaging system (manufactured by NT-MDT BV, Amsterdam, The Netherlands), which combines optical microscopy, AFM, and Raman spectroscopy. Scanning was performed in intermittent contact mode using NSG01 silicon probes (NT-MDT BV, Amsterdam, The Netherlands) with a tip curvature radius of ~10 nm and a resonant frequency in the range of 140–150 kHz. Surface analysis was performed at several scales: with scanning areas of 50 × 50 $\mu m^2$ and 20 × 20 $\mu m^2$, with a fixed resolution of 400 × 400 pixels. The scanning speed was 0.3 Hz, ensuring an optimal balance between measurement time and the quality of microstructural detail imaging.

AFM height profiles were used to evaluate the vertical dimension and aggregation state of the observed surface structures.

### 2.5. Bitumen Modification

Bitumen was poured into a metal beaker equipped with a thermometer and a heated stirrer. The beaker was heated to 140 ± 10 °C. The graphene oxide-like material (3 wt.%) was added to the heated bitumen at a dosage of 3 wt.% relative to the mass of bitumen. The mixture was stirred at 500–700 rpm for 1 h using a mechanical stirrer (IKA RW20, Königswinter, Germany) until a homogeneous binder was obtained. A dosage of 3 wt.% was selected based on studies in which this concentration provided a more pronounced improvement in the properties of GO-modified bitumen compared with lower concentrations [20]. In the present study 3 wt.% is therefore considered a selected modification dosage rather than an optimum dosage.

### 2.6. Bitumen Aging

To simulate prolonged oxidative aging of bitumen samples an extended Rolling Thin-Film Oven Test (RTFOT) procedure based on [25] was used. The apparatus consisted of a double-walled internal oven with circulating hot air, at a test temperature of 163 ± 0.5 °C, driven by an internal fan. Eight specially designed glass sample bottles were mounted horizontally on a carousel inside the oven. The test involved exposing a thin layer of bitumen (~1.25 mm) to a hot air jet for 225 min. Each modified bitumen sample, along with a reference bitumen without additives, was added at a rate of 35 ± 0.5 g to each of the glass containers to provide sufficient material for testing with the remaining samples. The samples were exposed to hot air for 225 min, which is longer than the standard RTFOT conditioning period and was therefore considered an extended aging procedure.

The exposure time of 225 min was selected based on the correlation reported in [26]. According to [26], prolonged RTFOT conditioning at 163 °C for 225 min was associated with approximately 10 years of field service under temperature climatic conditions. However, this relationship should be regarded as an approximate laboratory-to-field correlation rather than a direct equivalence.

### 2.7. Physico-Mechanical Testing of Bitumen

Penetration indirectly characterizes the hardness of bitumen and is determined by the depth of penetration of a standard needle under specified conditions. After conditioning at 25 °C for 1 h, the penetration was measured at 25 °C for 5 s under a load of 100 g using an APN-360MG4 (SKB Stroypribor LLC, Chelyabinsk, Russia) penetrometer in accordance with [27].

Softening point is the temperature at which bitumen changes from a relatively solid state to a softened state. The softening point was determined by the Ring and Ball method using a KISH-MG4 (SKB Stroypribor LLC, Chelyabinsk, Russia) apparatus. The samples were heated in a water bath at a rate of 5 ± 0.5 °C/min in accordance with [28].

Ductility characterizes the ability of bitumen to elongate before breaking and is determined by the length of the specimen at rupture. Ductility was measured using a DAF-1480 (VNIR, Moscow, Russia) ductilometer in accordance with [29].

### 2.8. LAS Test

To assess the fatigue strength of bituminous binders, a Linear Amplitude Sweep (LAS) test was conducted according to [30], based on the Viscoelastic Continuum Damage (VECD) model according to [31]. The tests were conducted on a SmartPave 102e (Anton Paar GmbH, Graz, Austria) rotational rheometer using 8 mm diameter parallel plate geometry at a temperature of 25 °C.

The test included two main stages. The first, Frequency Sweep, determined the linear viscoelastic properties of the specimen required for VECD calculations. Measurements were conducted at a fixed strain of 0.1% in a frequency range from 0.2 to 30 Hz.

The second stage, Amplitude Sweep, investigated the material's resistance to fatigue failure at increasing strain levels. The oscillation frequency remained constant (10 Hz), and the deformation amplitude increased uniformly from 0.1% to 30% over a specified number of steps. The LAS procedure provides an accelerated binder-level laboratory assessment of fatigue characteristics under cyclic shear loading and does not directly reproduce pavement traffic loading conditions.

The obtained data were processed in the RheoCompassTM 2.1 software environment. The following relationships and parameters were determined: damage curve C(S), fatigue life curve ($N_f$), key VECD model parameters ($C_0$, $C_i$, $C_2$, $\alpha$, $I_D$, $D_f$, k, A, and B), and the number of cycles to failure ($N_f$) at applied strain levels of 2.5%, 5%, 7.5%, 10%, and 15%.

All rheological tests were performed in triplicate. The reported values represent the arithmetic mean of three replicate measurements, and variability is expressed as the standard deviation (SD).

## 3. Results and Discussion

### 3.1. Structure of Graphene Oxide-like Material

Raman spectroscopy was used to evaluate the structural changes in graphene oxide-like material obtained from lemon peel biochar produced at different pyrolysis temperatures (500, 550 and 600 °C) and synthesized using a modified Hummers method. Raman spectroscopy is one of the most sensitive and informative methods for studying the structural features of carbon materials, including graphene oxide. It allows not only for the evaluation of carbon structural ordering but also for the assessment of the level of defects and tracking of structural changes during chemical modification [32].

The resulting spectra (Figure 3) clearly display two main bands, the D and G bands, commonly observed in defective and oxidized carbon materials. The D band (~1350 $cm^{-1}$) is associated with structural disorder in the carbon lattice. Its intensity can be influenced by defects and oxygen-containing functional groups (–OH, COOH, –C=O), which are typical for oxidized forms of carbon. The G band (~1580 $cm^{-1}$) corresponds to vibrations of C–C bonds in $sp^2$-hybridized structures and indicates the presence of regions that retain graphene-like ordering [33]. Additionally, a weak 2D peak reflecting double scattering processes is observed in the 2700–2900 $cm^{-1}$ region. Its relatively low intensity and shape are consistent with a defective and multilayered carbon structure [33].

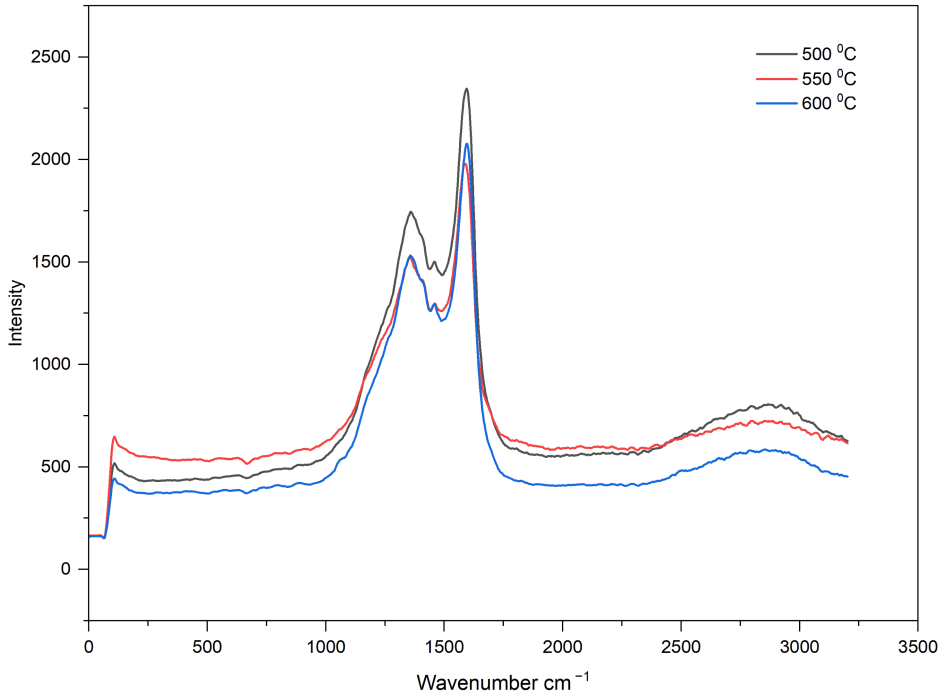


**Figure 3.** Raman spectra of GO-like material synthesized from lemon peel biochar at different pyrolysis temperatures.

The intensity ratio of these peaks ($I_D/I_G$) is approximately 0.7–0.75, indicating moderate defectiveness of the obtained structures of the synthesized graphene oxide-like material.

Based on a comparison of the spectra, it can be concluded that the temperature of the biomass pre-pyrolysis has a significant effect on the structure of the resulting graphene oxide-like material. The sample obtained at 550 °C exhibits the most balanced ratio between defects and structural order, suggesting that this temperature regime was the most

favorable among the investigated pyrolysis conditions based on structural characterization for graphene oxide-like material from lemon peel.

Figure 4 shows atomic force microscopy images (50 × 50 µm) and the height profiles of graphene oxide-like material synthesized by a modified Hummers method from biochar produced at different pyrolysis temperatures.

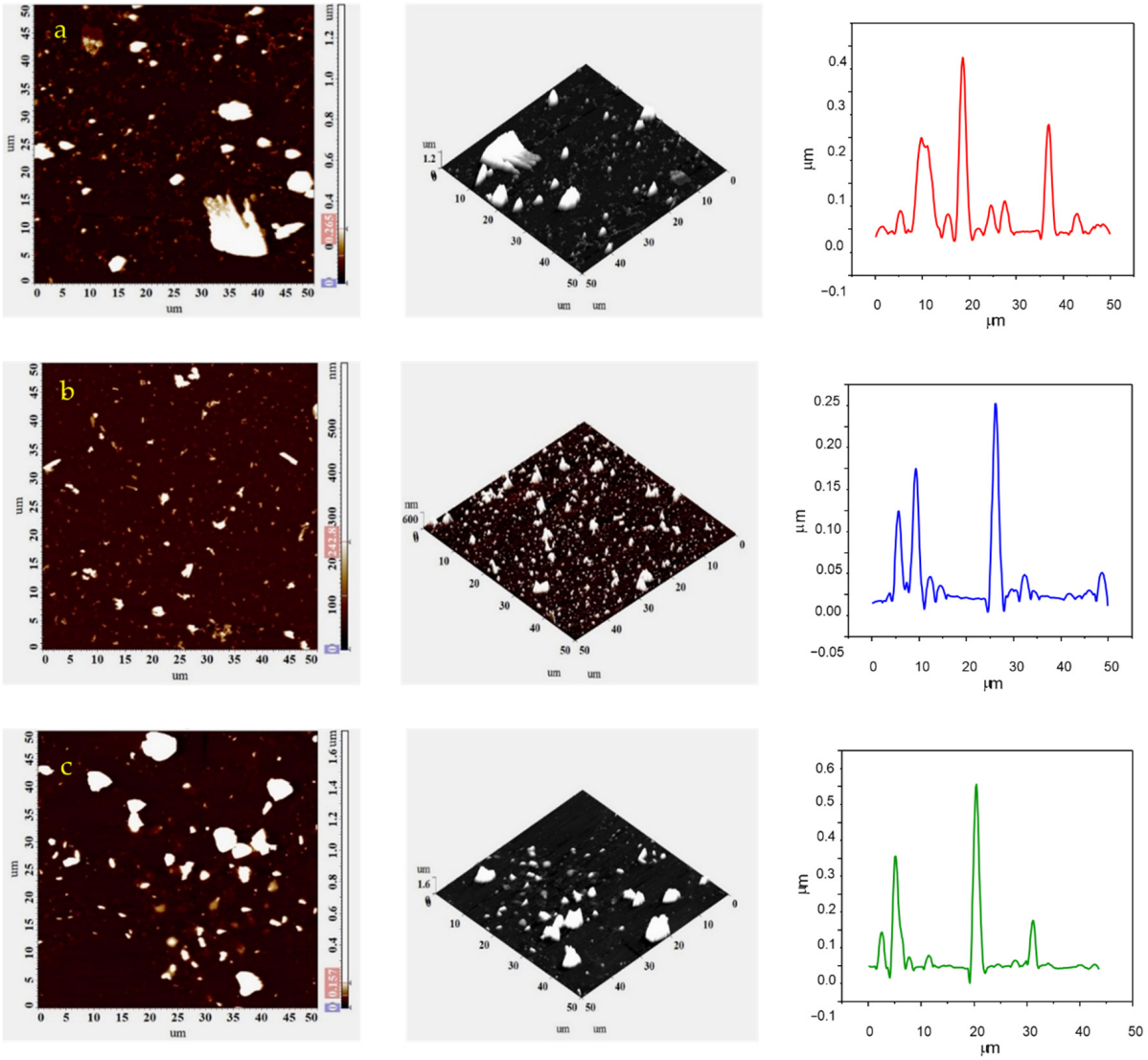


**Figure 4.** Atomic force microscopy images (50 × 50 µm) of graphene oxide-like material synthesized using a modified Hummers method from biochar obtained at different pyrolysis temperatures: (**a**) 500 °C, (**b**) 550 °C, (**c**) 600 °C.

Figure 4a (pyrolysis temperature of 500 °C) shows the presence of both relatively small and large fragments, with a maximum height of approximately 1.2 µm. The distribution of sheet-like structures is uneven, with visible agglomerations, indicating possible incomplete oxidative disintegration of the carbon matrix. This result may be due to the insufficient level of structural defects in the biochar obtained at a lower temperature, which may limit the incorporation of oxygen-containing functional groups into the carbon structure during the oxidation process.

Figure 4b (pyrolysis temperature of 550 °C) demonstrates a relatively uniform distribution of surface features over the scanned area. The AFM height of the observed structures is predominantly in the range of approximately 100–300 nm. The observed height range

may be associated with partial stacking and aggregation of sheet-like structures within the analyzed samples.

The surface is characterized by high heterogeneity, which may be due to the formation of thermally stable, poorly oxidized structures at elevated carbonization temperatures. These conditions promote the formation of a denser carbon lattice resistant to acidic oxidizing agents, which may complicate the effective cleavage of graphite layers.

The surface profile of the sample pre-treated at 550 °C shows AFM height variations predominantly in the range of approximately 20 to 250 nm. These values characterize the vertical dimensions of the observed surface features and may be influenced by local stacking and aggregation of the sheet-like structures.

The sample pre-treated at 500 °C exhibits more pronounced height variations, with individual peaks reaching ~500 nm. Along with nanoscale elements (100–200 nm), larger fragments are observed, which may be due to insufficient amorphization of the biochar and, consequently, incomplete disintegration during oxidation.

The sample obtained at 600 °C exhibits significant height variations—up to 650 nm—indicating the presence of large multilayer aggregates. Despite the presence of individual nanofragments, the overall structure of the material is highly heterogeneous and exhibits a tendency toward aggregation, which may be due to excessive thermal stabilization of the carbon lattice.

Thus, analysis of the height profile confirms that pyrolysis temperature has a significant influence on the morphological characteristics of graphene oxide-like carbon material. The most favorable structure, with a predominance of dispersed sheet-like structures, was observed at 550 °C.

Figure 5 shows the IR spectra of graphene oxide-like material samples synthesized from lemon peel biochar obtained by pyrolysis at different temperatures. All spectra retain the same set of absorption bands, but their intensity and shape vary depending on the heat treatment temperature.

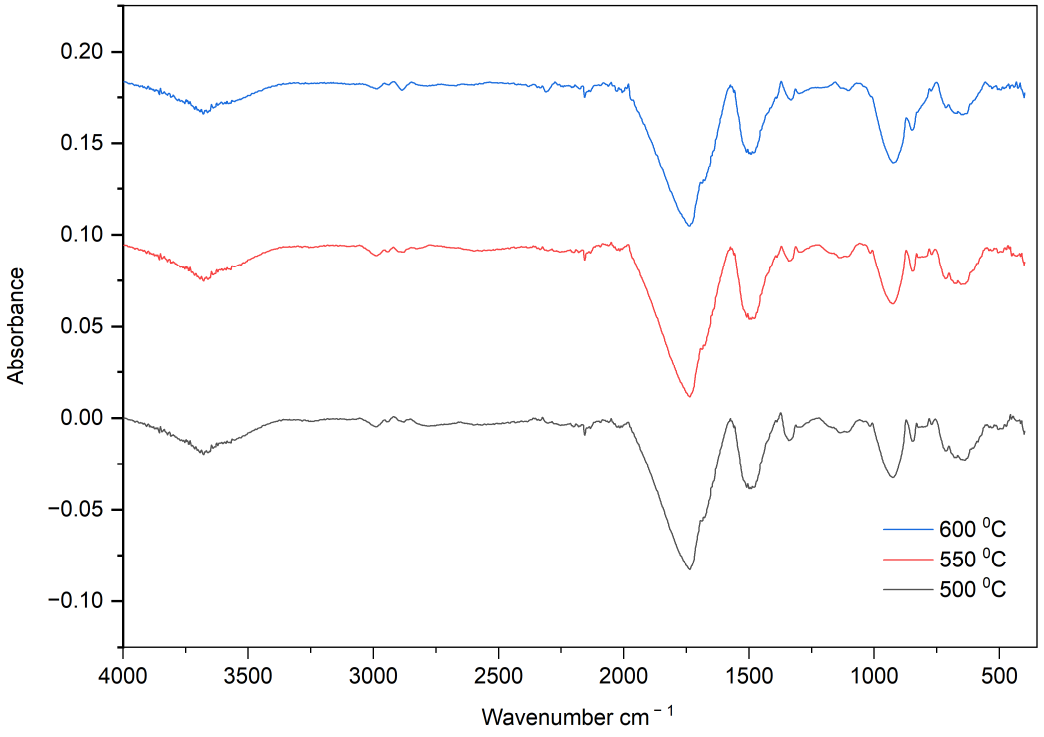


**Figure 5.** FTIR spectra of GO-like material produced from lemon peel biochar at different pyrolysis temperatures.

The broad band at 3400 $cm^{-1}$ corresponds to the stretching vibrations of O–H groups. Its maximum intensity is observed at 550 °C, while at lower or higher temperatures, the intensity decreases. The band at 1720 $cm^{-1}$, corresponding to vibrations of carbonyl C=O groups, is also most intense at 550 °C.

In the range of 1050–1200 $cm^{-1}$, C–O vibration bands (alcohols, ethers, epoxy groups) are observed, and their maximum intensity is also reached at 550 °C.

Thus, analysis of the IR spectra shows that the highest relative contribution of oxygen-containing functional groups (O–H, C=O, C–O) was observed for the sample obtained at 550 °C, indicating that this temperature is the most favorable among the investigated conditions for producing highly functional graphene oxide-like material.

### *3.2. Bitumen Modification Results*

To evaluate the performance of GO-like material modified bitumen after prolonged aging, a comparative analysis was conducted between bitumen samples aged using the RTFOT method for 225 min: the neat (without additives) and the bitumen with the 3 wt.% graphene oxide-like material.

Table 1 shows the physical characteristics of samples of bitumen BND 100/130 and bitumen modified with 3 wt.% GO-like material before and after aging. According to the table, the addition of 3 wt.% GO-like material alters the standard physical and mechanical properties of bitumen. For unaged modified bitumen, the softening point increases from 46.9 ± 0.3 to 56.7 ± 0.3 °C, and penetration decreases from (129.6 ± 0.1)·0.1 mm to (119.2 ± 0.9)·0.1 mm, indicating an increase in binder stiffness. At the same time, ductility decreases from 111.6 ± 1.0 to 51.2 ± 0.8 cm.

**Table 1.** Physico-mechanical properties of neat and 3 wt.% GO-like material modified BND 100/130 bitumen before and after aging.

| Sample | Softening Point, °C | Penetration at 25 °C, 0.1 mm | Ductility at 25 °C, cm |
|---|---|---|---|
| Neat bitumen | 46.9 ± 0.3 | 129.6 ± 0.1 | 111.6 ± 1.0 |
| Bitumen modified with 3 wt.% GO-like material | 56.7 ± 0.3 | 119.2 ± 0.9 | 51.2 ± 0.8 |
| Aged neat bitumen | 47.6 ± 0.3 | 42.0 ± 0.8 | 54.4 ± 0.4 |
| Aged bitumen modified with 3 wt.% GO-like material | 55.4 ± 0.4 | 45.6 ± 0.5 | 109.4 ± 1.2 |

After laboratory aging, the differences between the samples persist. The softening point of the modified bitumen is 55.4 ± 0.4 °C, compared to 47.6 ± 0.3 °C for the aged neat bitumen. Penetration is (45.6 + 0.5)·0.1 mm and (42.0 + 0.8)·0.1 mm, respectively, while the ductility of the modified sample reaches 109.4 + 1.2 cm versus 54.4 + 0.4 cm for the aged neat bitumen. Thus, after aging, the modified bitumen is characterized by a higher softening point and retains higher deformability compared to the aged neat bitumen.

Figure 6 shows the dependence of effective shear stress on effective shear strain for two bitumen samples: the neat bitumen subjected to thermal-oxidative aging using the RTFOT method for 225 min, and the modified bitumen with the addition of 3% graphene oxide-like material, which underwent a similar heat treatment. The figure shows that the modified bitumen exhibits higher maximum stress (~145–150 kPa versus ~120–125 kPa for the unmodified bitumen), an increase in the ultimate effective shear strain from approximately 13% to 17% and more stable behavior after reaching the peak, indicating increased strength and ductility.

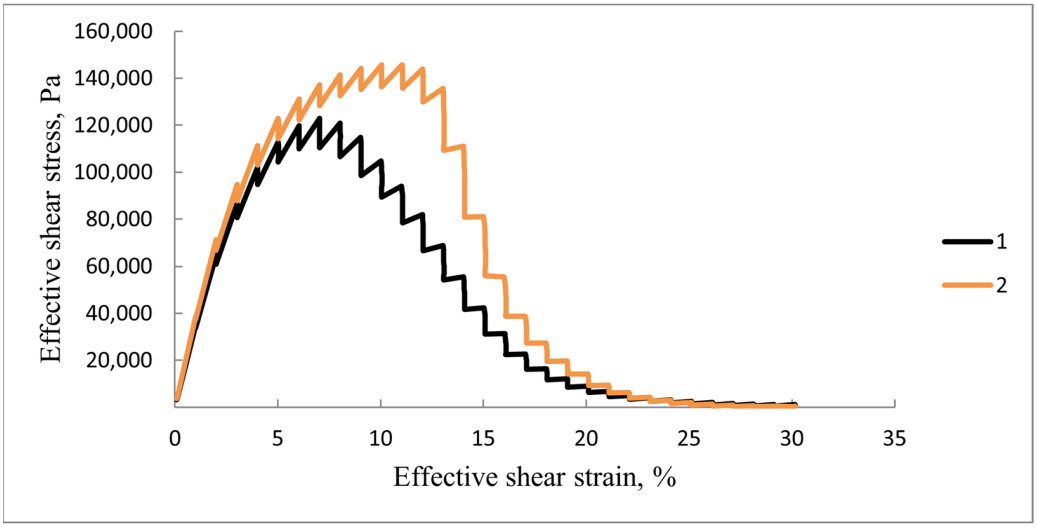


**Figure 6.** Effective shear stress versus effective shear strain for aged neat bitumen (1) and aged bitumen modified with 3 wt.% GO-like material (2).

Figure 7 shows damage curves obtained using the VECD model based on the amplitude shear test for bitumen aged using the RTFOT method for 225 min, as well as for the same bitumen modified with 3 wt.% graphene oxide-like material. An analysis of the curves shows that the modified bitumen exhibits higher damage function C values at the same damage intensity compared to the neat modified sample. Damage function C characterizes the decrease in residual stiffness of the bitumen binder as the intensity of accumulated damage increases. This indicates a slower decrease in material stiffness and a delay in structural degradation processes. Thus, modified bitumen exhibits greater resistance to damage accumulation and failure under cyclic loading.

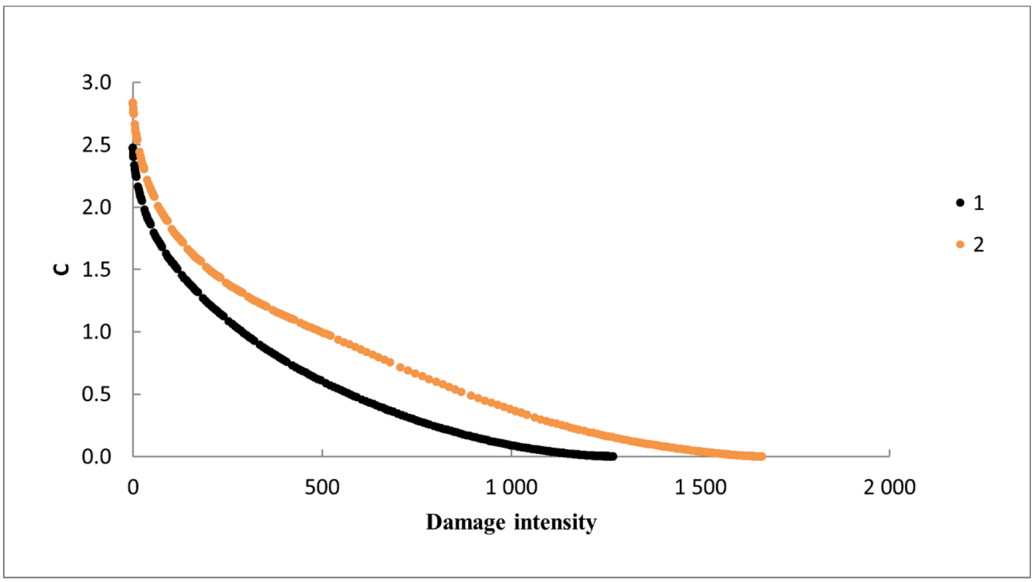


**Figure 7.** VECD damage curves plotted based on the results of the amplitude shear test for aged neat bitumen (1) and aged bitumen modified with 3 wt.% GO-like material (2).

Furthermore, the modified specimen maintains its performance over a wider range of damage intensities, indicating improved mechanical properties. This effect may be associated with the reinforcing and stabilizing influence of graphene oxide-like material, which may contribute to maintaining a more stable internal structure of the bitumen after prolonged aging.

Figure 8 and Table 2 show the dependence of the fatigue life of bitumen binders on the strain level, obtained using the LAS test within the VECD model. The comparison was made between bitumen artificially aged using the RTFOT method for 225 min and a bitumen modified with 3 wt.% GO-like material that underwent similar thermal-oxidative treatment.

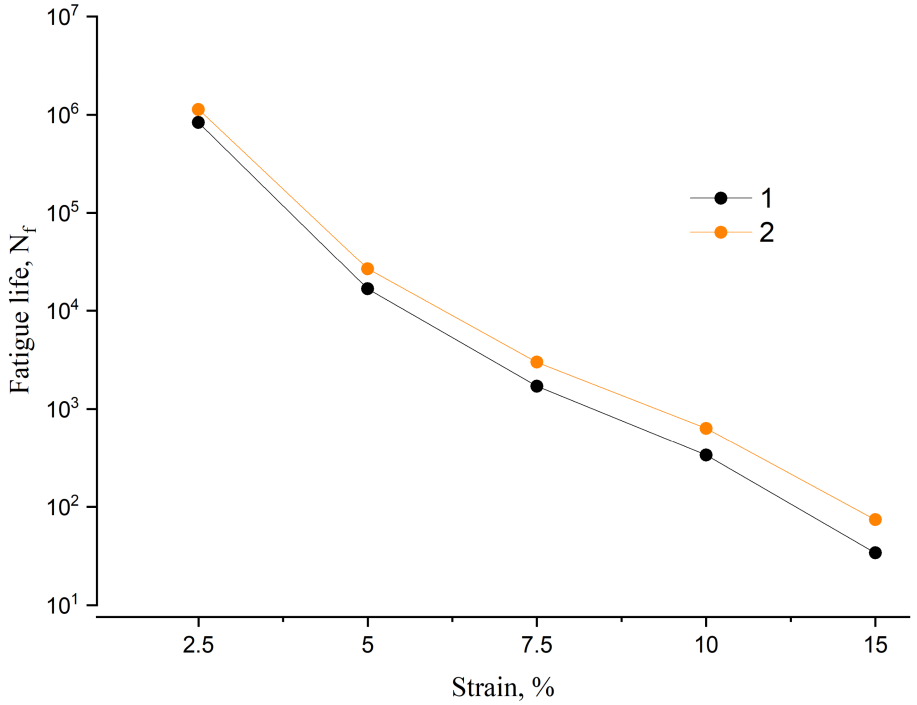


**Figure 8.** Dependence of fatigue life on strain level for aged neat bitumen (1) and aged bitumen modified with 3 wt.% GO-like material (2).

**Table 2.** Fatigue life of aged neat bitumen and 3 wt.% GO-like material modified aged bitumen at different strain levels.

| Strain, % | Number of Cycles to Failure of Aged Neat Bitumen, $N_f$ | Number of Cycles to Failure of Aged Bitumen Modified with 3 wt.% GO-like Material, $N_f$ |
|---|---|---|
| 2.5 | 831,766 ± 12,967 | 1,131,422 ± 70,688 |
| 5 | 16,762 ± 2554 | 26,779 ± 1182 |
| 7.5 | 1708 ± 351 | 2997 ± 173 |
| 10 | 338 ± 85 | 634 ± 32 |
| 15 | 34 ± 13 | 71 ± 8 |

The LAS test results also demonstrate an increase in fatigue life (the number of cycles to failure, $N_f$) at all strain levels. At the 2.5% strain level, the modified specimen shows a 36% increase in $N_f$ (from ~831,766 to ~1,131,422 cycles); at 5%, a 60% increase; and at 15%, a more than twofold increase (from 34 to 71 cycles). This indicates increased resistance to fatigue failure, even after prolonged laboratory aging.

Table 3 presents the key VECD model parameters obtained for the aged neat bitumen and aged modified bitumen. The modified binder showed higher values of $C_0$, $C_i$, $I_D$, $D_f$, k, and A, whereas slightly lower values were observed for $C_2$, $\alpha$, and B. Overall, these results indicate that the incorporation of GO-like material affects the damage evolution characteristics of the binder and is consistent with the improved fatigue performance observed in the LAS-test.

**Table 3.** Key VECD model parameters for aged neat bitumen and bitumen modified with 3 wt.% GO-like material.

| Parameters | Aged Bitumen | Aged Bitumen Modified with 3 wt.% GO-like Material |
|---|---|---|
| $C_0$ | 2.474 ± 0.001 | 2.755 ± 0.001 |
| $C_1$ | 0.169 ± 0.001 | 0.172 ± 0.001 |
| $C_2$ | 0.380 ± 0.003 | 0.377 ± 0.005 |
| α | 2.816 ± 0.015 | 2.804 ± 0.013 |
| $I_D$ (MPa) | 3.464 ± 0.022 | 3.841 ± 0.019 |
| $D_f$ | 406 ± 3 | 552 ± 4 |
| k | 2.746 ± 0.001 | 2.748 ± 0.002 |
| A | (1.451 ± 0.008)·$10^8$ | (1.482 ± 0.005)·$10^8$ |
| B | 5.633 ± 0.127 | 5.608 ± 0.098 |

Thus, the addition of GO-like material improves the rheological and mechanical properties of bitumen after prolonged aging and results in a higher fatigue resistance under cyclic loading. Adding 3 wt.% graphene oxide-like material to bitumen improves its properties, which may be associated with a reinforcing and stabilizing effect within the matrix.

It should be noted that the study focused on a single modifier dosage of 3 wt.%, so the obtained results relate specifically to this concentration. The evaluation was conducted primarily on aged samples, allowing for a comparison of their properties after laboratory aging.

An extended RTFOT procedure was used for aging. The structural properties of the synthesized material were evaluated using Raman, FTIR, and AFM. Recent research also demonstrates the potential of agricultural byproducts as bitumen modifiers. Agricultural byproducts and biowastes have been investigated as bio-rejuvenators for aged bitumen binders [34].

The obtained results are generally consistent with previous studies of GO-modified bitumen. The effectiveness of GO depends on its dosage, bitumen type, preparation conditions, and dispersion [21]. In this study, the introduction of 3 wt.% GO-like material increased the fatigue life at all strain levels studied. Similar trends have also been observed in previous studies using the LAS test [19].

A distinctive feature of this study is the use of a material obtained from lemon peel biochar instead of traditional graphitic GO. Differences in the structure and imperfections of biomass-derived materials can affect their dispersion and interaction with bitumen.

The use of renewable biomass feedstocks is of interest for waste recycling and the production of functional carbon materials. However, to more fully assess the sustainability of this approach, it is advisable to consider reagent consumption and energy costs, as well as wastewater generation, which were not evaluated in the present study and should be addressed in future research.

## 4. Conclusions

The study found that the pyrolysis temperature of lemon peel significantly affects the structural and morphological characteristics of graphene oxide-like (GO-like) material synthesized using a modified Hummers method. Among the investigated temperatures 550 °C was the most favorable based on structural characterization for preliminary heat treatment of the raw material. This temperature provides the most favorable relationship between defects to structural order ($I_D/I_G \approx 0.7$–$0.75$), the highest relative contribution of oxygen-containing functional groups (–OH, C=O, C–O), and the most uniform distribution of sheet-like structures with AFM height values predominantly in the range of 100–300 nm.

It has been shown that the addition of the selected dosage of 3 wt.% GO-like material to the bitumen binder improves its rheological and mechanical properties: effective shear stress increases by approximately 20–25 kPa, ultimate strain increases from 13% to 17%, and fatigue life increases by approximately 36–109%, depending on the strain level. These results indicate improved rheological and fatigue performance of the modified binder after prolonged thermal-oxidative aging. The results confirm the potential of using lemon peel as a renewable raw material for producing functional carbon nanomaterials effective for modifying road bitumen.

**Author Contributions:** Conceptualization, A.K. and Y.O.; methodology, A.K.; software, A.K.; validation, A.K.; formal analysis, A.K.; investigation, A.K.; resources, A.K.; data curation, A.K.; writing—original draft preparation, A.K.; writing—review and editing, Y.O.; visualization, Y.O.; supervision, Y.O.; project administration, A.K.; funding acquisition, A.K. All authors have read and agreed to the published version of the manuscript.

**Funding:** This research was funded by the Science Committee of the Ministry of Science and Higher Education of the Republic of Kazakhstan, grant No. AP25795719, "Developing a bitumen modifying technology with a solid pyrolysis product of used tires and food waste to impart antioxidant properties".

**Data Availability Statement:** The raw data supporting the conclusions of this article will be made available by the authors on request.

**Conflicts of Interest:** The authors declare no conflicts of interest.

## References

1. Lesueur, D. The Colloidal Structure of Bitumen: Consequences on the Rheology and on the Mechanisms of Bitumen Modification. *Adv. Colloid Interface Sci.* **2009**, *145*, 42–82. [CrossRef] [PubMed]
2. Huang, H.; Wang, Y.; Wu, X.; Zhang, J.; Huang, X. Nanomaterials for Modified Asphalt and Their Effects on Viscosity Characteristics: A Comprehensive Review. *Nanomaterials* **2024**, *14*, 1503. [CrossRef] [PubMed]
3. Xing, C.; Han, Z.; Li, M.; Zhu, B.; Sun, Z.; Wang, Y.; Wang, S. Thermal History-Induced Nanoscale Surface Characteristics of Bitumen: Implications of Sample Preparation on Accurate Characterization. *Appl. Surf. Sci.* **2026**, *730*, 166309. [CrossRef]
4. Habib, N.; Ng, C.; Zoorob, S.; Lee, P. Use of Graphene Oxide as a Bitumen Modifier: An Innovative Process Optimization Study. *Adv. Mater. Res.* **2015**, *1105*, 365–369. [CrossRef]
5. Zhu, J.; Zhang, K.; Liu, K.; Shi, X. Adhesion Characteristics of Graphene Oxide Modified Asphalt Unveiled by Surface Free Energy and AFM-Scanned Micro-Morphology. *Constr. Build. Mater.* **2020**, *244*, 118404. [CrossRef]
6. Zeng, Q.; Liu, Y.; Liu, Q.; Liu, P.; He, Y.; Zeng, Y. Preparation and Modification Mechanism Analysis of Graphene Oxide Modified Asphalts. *Constr. Build. Mater.* **2020**, *238*, 117706. [CrossRef]
7. Liu, K.; Zhu, J.; Zhang, K.; Wu, J.; Yin, J.; Shi, X. Effects of Mixing Sequence on Mechanical Properties of Graphene Oxide and Warm Mix Additive Composite Modified Asphalt Binder. *Constr. Build. Mater.* **2019**, *217*, 301–309. [CrossRef]
8. Marcano, D.C.; Kosynkin, D.V.; Berlin, J.M.; Sinitskii, A.; Sun, Z.; Slesarev, A.S.; Alemany, L.B.; Lu, W.; Tour, J.M. Improved Synthesis of Graphene Oxide. *ACS Nano* **2010**, *4*, 4806–4814. [CrossRef] [PubMed]
9. Dreyer, D.; Park, S.; Bielawski, C.; Ruoff, R. The Chemistry of Graphene Oxide. *Chem. Soc. Rev.* **2009**, *39*, 228–240. [CrossRef] [PubMed]
10. Biswal, B.K.; Balasubramanian, R. Biomass-Derived Carbon as Sustainable Materials for Application in Clean Energy Storage Technologies: Progress and Outlook. *Carbon* **2026**, *246*, 120931. [CrossRef]
11. De Rose, E.; Bartucci, S.; Poselle Bonaventura, C.; Conte, G.; Agostino, R.G.; Policicchio, A. Effects of Activation Temperature and Time on Porosity Features of Activated Carbons Derived from Lemon Peel and Preliminary Hydrogen Adsorption Tests. *Colloids Surf. A Physicochem. Eng. Asp.* **2023**, *672*, 131727. [CrossRef]
12. Ozcan, O.; Yumrutas, H.I.; Gedik, A.; Ozcanan, S.; Apak, M.Y. Assessing the Potential of Olive Stone Powder as a Bitumen Biopolymer Through Physical, Chemical, and Rheological Characterization. *Polymers* **2026**, *18*, 661. [CrossRef] [PubMed]
13. Surya, K.; Michael, M.S. Hierarchical Porous Activated Carbon Prepared from Biowaste of Lemon Peel for Electrochemical Double Layer Capacitors. *Biomass Bioenergy* **2021**, *152*, 106175. [CrossRef]
14. Weldekidan, H.; Patel, H.; Mohanty, A.; Misra, M. Synthesis of Porous and Activated Carbon from Lemon Peel Waste for $CO_2$ Adsorption. *Carbon Capture Sci. Technol.* **2024**, *10*, 100149. [CrossRef]

15. Fang, Z.; Gao, Y.; Bolan, N.; Shaheen, S.M.; Xu, S.; Wu, X.; Xu, X.; Hu, H.; Lin, J.; Zhang, F.; et al. Conversion of Biological Solid Waste to Graphene-Containing Biochar for Water Remediation: A Critical Review. *Chem. Eng. J.* **2020**, *390*, 124611. [CrossRef]
16. Rizianiza, I.; Kusrini, E.; Siswantara, A.I.; Aziz, M.; Ivo, P.; Maknun, I.J.; Ichsan, R.R.; Khoiro Ummatin, K.; Usman, A. Biomass-Derived Biochar as a Precursor for Graphene-like Carbon Materials via Slow Pyrolysis: A Review. *J. Environ. Chem. Eng.* **2026**, *14*, 122685. [CrossRef]
17. Singh, D.; Kuity, A.; Girimath, S.; Suchismita, A.; Showkat, B. Investigation of Chemical, Microstructural, and Rheological Perspective of Asphalt Binder Modified with Graphene Oxide. *J. Mater. Civ. Eng.* **2020**, *32*, 4020323. [CrossRef]
18. Peng, X.; Pan, F.; Lin, Z.; Lv, S.; Liu, P. Experimental and Molecular Dynamics Investigation of Graphene Oxide-Modified Bio-Oil Rejuvenated Asphalt Binder. *Constr. Build. Mater.* **2025**, *494*, 143354. [CrossRef]
19. Adnan, A.M.; Lü, C.; Luo, X.; Wang, J. Impact of Graphene Oxide on Zero Shear Viscosity, Fatigue Life and Low-Temperature Properties of Asphalt Binder. *Materials* **2021**, *14*, 3073. [CrossRef] [PubMed]
20. Wu, S.; Zhao, Z.; Li, Y.; Pang, L.; Amirkhanian, S.; Riara, M. Evaluation of Aging Resistance of Graphene Oxide Modified Asphalt. *Appl. Sci.* **2017**, *7*, 702. [CrossRef]
21. He, J.; Hu, W.; Xiao, R.; Wang, Y.; Polaczyk, P.; Huang, B. A Review on Graphene/GNPs/GO Modified Asphalt. *Constr. Build. Mater.* **2022**, *330*, 127222. [CrossRef]
22. Safian, M.; Haron, U.; Ibrahim, M. A Review on Bio-Based Graphene Derived from Biomass Wastes. *BioResources* **2020**, *15*, 9756–9785. [CrossRef]
23. Alhassan, H.; Yoong, V.N.; Soon, Y.W.; Usman, A.; Bakar, M.S.A.; Ahmed, A.; Luengchavanon, M. The Differential Influence of Biochar and Graphite Precursors on the Structural, Optical, and Electrochemical Properties of Graphene Oxide. *Mater. Chem. Phys.* **2025**, *329*, 130070. [CrossRef]
24. Hummers, W.S.J.; Offeman, R.E. Preparation of Graphitic Oxide. *J. Am. Chem. Soc.* **1958**, *80*, 1339. [CrossRef]
25. *ASTM D2872-04*; Standard Test Method for Effect of Heat and Air on a Moving Film of Asphalt (Rolling Thin-Film Oven Test). ASTM (American Society for Testing and Materials): West Conshohocken, PA, USA, 2012.
26. Gargiulo, V.; Alfe, M.; Ruoppolo, G.; Cammarota, F.; Rossi, C.O.; Loise, V.; Porto, M.; Calandra, P.; Pochylski, M.; Gapinski, J. How Char from Waste Pyrolysis Can Improve Bitumen Characteristics and Induce Anti-Aging Effects. *Colloids Surf. A Physicochem. Eng. Asp.* **2023**, *676*, 132199. [CrossRef]
27. *ST RK 1226-2003*; Bitumens and Bituminous Binders. Method for Determining the Depth of Needle Penetration. Kazstandard: Astana, Kazakhstan, 2003.
28. *ST RK 1227-2003*; Bitumens and Bituminous Binders. Determination of Softening Point by the Ring and Ball Method. Kazstandard: Astana, Kazakhstan, 2003.
29. *ST RK 1374-2005*; Bitumens and Bituminous Binders. Method for Determining Ductility. Kazstandard: Astana, Kazakhstan, 2005.
30. *AASHTO T391-20*; Estimating Fatigue Resistance of Asphalt Binders Using the Linear Amplitude Sweep. American Association of State Highway and Transportation Officials (AASHTO): Washington, DC, USA, 2021.
31. *AASHTO TP101-14*; Standard Method of Test For Estimating Damage Tolerance of Asphalt Binders Using The Linear Amplitude Sweep. American Association of State Highway and Transportation Officials (AASHTO): Washington, DC, USA, 2014.
32. Ferrari, A.C.; Meyer, J.; Scardaci, V.; Casiraghi, C.; Lazzeri, M.; Mauri, F.; Piscanec, S.; Jiang, D.; Novoselov, K.; Roth, S. Raman Spectrum of Graphene and Graphene Layers. *Phys. Rev. Lett.* **2006**, *97*, 187401. [CrossRef] [PubMed]
33. Sparavigna, A.C. Graphene and Graphene Oxide (Raman Spectroscopy). *ChemRxiv* **2024**. [CrossRef]
34. Pimenta, M.; Dresselhaus, G.; Dresselhaus, M.; Cançado, L.; Jorio, A.; Saito, R. Studying Disorder in Graphite-Based Systems by Raman Spectroscopy. *Phys. Chem. Chem. Phys.* **2007**, *9*, 1276–1291. [CrossRef] [PubMed]